ISSN 1069-3513, Izvestiya, Physics of the Solid Earth, 2020, Vol. 56, No. 3, pp. 337–356. © Pleiades Publishing, Ltd., 2020.
Russian Text © The Author(s), 2020, published in Fizika Zemli, 2020, No. 3, pp. 52–73.

Spatiotemporal Variations in Gutenberg–Richter *b*-Value Depending on the Depth and Lateral Position in the Earth's Crust of the Garm Region, Tajikistan

G. A. Popandopoulos*

Schmidt Institute of Physics of the Earth, Russian Academy of Sciences, Moscow, 123242 Russia
**e-mail: gap@ifz.ru*

Received March 11, 2019; revised September 8, 2019; accepted October 7, 2019

Abstract—Spatiotemporal variations in the Gutenberg–Richter (GR) *b*-value and in the minimum magnitude of a predicted earthquake (*MPE*) are studied in detail depending on the depth and lateral position of the selected sample of earthquakes in the Garm region, Tajikistan. The time variations in *b*-value estimated from the data on the earthquakes in the different depth intervals indicate that most of the "strong" events with $M \geq MPE$ were preceded by the significant time anomalies localized in the vicinity of the source depths of these earthquakes. The maximum amplitudes of these anomalies gravitate to the vicinity of the hypocenters of the strong earthquakes and decay with distance from the hypocenter. The observed time anomalies in the *b*-value, which have a shape of a positive bay, are not accidental, which is demonstrated by their sufficient statistical representativeness (18 events). It is concluded that based on the used approach it will be possible to estimate the source depth of a future strong earthquake. The estimate of earthquake prediction quality based on 38 "strong" earthquakes with $M \geq MPE$ that occurred in seven local regions during a 23-year observation period shows that in 84% of cases, the emergence of *b*-value anomalies is accompanied by the successful forecasts. At the same time, the overall probability estimate of a medium-term forecast of the "strong" earthquakes with false alarms and missed events taken into account is 71%. Meanwhile, the forecasting quality of the strong earthquakes substantially increases if the *b*-value time variations are monitored separately in the different depth intervals of the Earth's crust. It is shown that the parameter of the minimum *MPE* estimated from the rightmost part of the linear segment of GR relationship is a characteristic of the structural blocks of the Earth's crust and varies both across the area and along the depth. It is hypothesized that the front of the deformation waves emerging on certain time intervals in a number of the local regions of the sample has probably been detected. The supposed deformation waves propagate with the velocities of 40–50 km/yr with their front moving NE to SE.The results of the study can be used for medium-term forecasting of the earthquakes with $M \geq MPE$, for estimating the depth of the expected earthquake, and for overall seismic hazard assessment in the seismically active regions.

Keywords: Gutenberg–Richter law, *b*-value time variations, positive bay-like anomalies, detection of a front of deformation waves

DOI: 10.1134/S1069351320020081

1. INTRODUCTION

The relationship between the magnitudes of the earthquakes and the frequency of their occurrence is one of the remarkable laws in seismology which make it possible to study the physical processes taking place in the Earth's crust. This relationship was discovered by the Japanese and American scientists who published in the middle of the 20th century their observations on the frequency–magnitude distribution (FMD) of the earthquakes (Ishimoto and Iida, 1939; Gutenberg and Richter, 1944). Subsequently, this relationship was called the Gutenberg–Richter (GR) law. This relationship has a simple and clear representation on the logarithmic scale:

$$\log N = a - bM, \quad (1)$$

where $\log N$ is the logarithm of the number of earthquakes with magnitudes M (or at least M in the case of cumulative distribution), and parameters a and b are equation constants referred to as the a- and b-value, respectively. The a-value characterizes the degree of seismic activity of the observation region or the productivity of the studied sample's size whereas b-value is the slope of the linear part of the GR distribution.

From the physical standpoint, b-value reflects the degree of the change in the number of earthquakes of small and large magnitudes in a given time interval within a fixed area. From the GR relationship it follows that high b-values characterize the relatively small number of earthquakes of large magnitudes and, correspondingly, low b-values testify to the opposite, i.e., to a relatively large number of earthquakes of large

magnitudes. Since the magnitude of the earthquakes is proportional to the length of the faults, it was shown by many authors that the *b*-value characterizes both the degree of heterogeneity of the medium and the relative intensity of tectonic stresses (Mogi, 1962; Scholz, 1968; Mori and Abercrombie, 1997; Schorlemmer et al., 2004a; 2004c; 2005; Popandopulo and Baskoutas, 2011; Popandopulo and Lukk, 2014; Baskoutas and Popandopoulos, 2014; Popandopulo, 2018).

The development of seismic observation networks and the increase in the determination accuracy of earthquakes' parameters aroused interest in *b*-value mapping over the area and along the depth of the Earth's crust (Mori and Abercrombie, 1997; Wiermer and Wyss, 1998; Gerstenberger et al., 2001; Zhu et al., 2005; Wyss and Stefansson, 2006; Wyss et al., 2008; Popandopulo and Lukk, 2014; Popandopoulos and Chatziioannou, 2014; Spada et al., 2013; Scholz, 2015; Popandopulo et al., 2016). In these studies, the depth changes in the *b*-value were considered in the context of the spatial heterogeneity of the medium. As a rule, it was observed that *b*-value decreases down to a depth of 8–15 km and increases with the further increase in depth.

The results of three-dimensional (3D) spatial mapping of *b*-value based on highly accurate seismological observations in the Garm region, Tajikistan, were published in (Popandopulo and Lukk, 2014). The cited study revealed two horizons with different trends of *b*-value behavior with depth above and below a depth of 15–16 km. In the upper horizon, *b*-value mainly decreases reaching minimum (0.8) close to a depth of 15–16 km. In the lower horizon, *b*-value generally increases with depth; its average value fluctuates within 1.2. It was established that in the lower horizon below 15 km the earthquakes with $M \geq 3.0$ were practically absent. It was found that the observed changes in *b*-value are determined by the ratio of the numbers of weak $M \geq 1.8$ and moderate $M \geq 3.0$ earthquakes at different depths. Considering the sufficient statistical significance of the results and high accuracy of hypocenters' determination, the authors of the cited work concluded that the observed changes in *b*-value with depth are not accidental.

Using the same catalog of the Garm earthquakes, Popandopulo (2018) analyzed the time variations in the *b*-value in order to reveal the pattern of their behavior before strong earthquakes. It was shown that in most cases, the strong earthquakes with magnitudes above the minimum magnitude of the predicted earthquake (*MPE*) are preceded by the bay-like convex variations in this parameter exceeding the threshold of statistical significance. In the cited paper, also the phenomenological model of the preparation of strong earthquakes explaining the time behavior of *b*-value was proposed.

This work logically continues the study of the regularity in the time behavior of *b*-value published in (Popandopoulos, 2018) for exploring the geodynamics of the Earth's crust and forecasting the strong earthquakes. The purpose of this work is to try to expand our understanding of the properties of *b*-value as a function of the depth and lateral strike of the local regions (LR) spanned by the sample. In addition, based on the analysis of the space position of the LRs it is possible to study the probable manifestations of deformation waves in the Earth's crust caused by the migration of the sources of the weak earthquakes. As previously, this work uses the catalog of the earthquakes recorded by the seismic network of the Complex Geophysical Expedition (CGE) of the Schmidt Institute of Physics of the Earth of the USSR Academy of Sciences which was operating at the Garm geodynamic testing site in Tajikistan from 1955 to 1992.

2. STUDY REGION AND OBSERVATION SYSTEM

The Garm region is located in the junction zone of two largest mountain systems—the Pamirs and the Tien Shan (Fig. 1). From the geological standpoint, the region under study includes the adjacent parts of the Pamir and Tien Shan separated by the Tajik Depression. These structural elements are expressed in the form of two largest fault zones—the Gissar–Kokshal zone in the north and the Darvaz–Karakul zone in the south of the region (Lukk and Shevchenko, 1990; Hamburger, 1992).

The seismological observations at the Garm geodynamic testing site were started in January 1955 when seven permanent seismic stations were installed there. From 1967 to 1992, 15 permanent recording stations were operating at the testing site. The seismological observations covered an area of approximately 120 × 60 km and the average distance between stations was 10–15 km. The created system for recording the local earthquakes provided the earthquake location accuracy at the center of the study area up to 1–15 km for the epicenters and up to 2–3 km for the source depth (Popandopulo, 1991).

In total, 93035 earthquakes were recorded during the period of seismological observations at the Garm testing site. All the earthquakes' seismograms were simultaneously processed by a single team of the researchers guided by T.F. Kotlyar, and the main parameters of the earthquakes were determined by a unified algorithm (Popandopoulos, 1991). The consistent processing of seismological data throughout the entire observation period and the use of a unified processing algorithm make the earthquake catalog obtained in CSE highly pertinent for studying seismic processes. These features of the catalog data are especially important for studying fine details such as, e.g., time variations in *b*-value depending on the source depth of the earthquake and spatial location of the local region (LR) of the sample of events under study.

Fig. 1. Tectonic elements and seismological observation system at Garm geodynamic test site of CGE IPE USSR Acad. Sci. Triangles with numbers are seismic stations. Small circles are epicenters of earthquakes with $M \geq 0.5$ that occurred from January 1, 1955 to March 31, 1992. The box in center is Kaudal local region (LR) considered for studying time variations in *b*-value with depth.

Figure 1 shows the spatial distribution of all the earthquakes with $M \geq 0.5$ that occurred from 1955 to 1992 (hereinafter M denotes local magnitude Ml). More detailed information on the study area, observation system and processing procedure are presented in (Lukk and Popandopoulos, 2012; Popandopoulos and Lukk, 2014; Popandopoulos, 2018). In particular, in these works it was shown that, within the observation system, the most uniform earthquake data with a minimum magnitude of completeness $Mc \approx 1.0$ are in the time interval from 1967 to 1992.

3. THE TECHNIQUE FOR CALCULATING THE *b*-VALUE AND CONSTRUCTION OF TIME SERIES

For calculating the selected *b*-values and for constructing the time series, the FastBEE program (Popandopoulos and Baskoutas, 2009) was used.

The *b-value* is calculated by the well–known Aki's formula (Aki, 1965) using the maximum likelihood method:

$$b(t) = \frac{\log e}{\bar{M}(t) - (Mc - \Delta M/2)}, \qquad (2)$$

where $\log e$ is a constant, Mc is the minimum magnitude of completeness, and $\bar{M}(t)$ is the mean magnitude of the earthquakes obtained from the earthquake sample in the averaging time window w, for $M \geq Mc$; ΔM is the magnitude bin, in our case $\Delta M = 0.1$. The root mean square error of *b*-value is calculated by the modified formula proposed in (Shi and Bolt, 1982):

$$\sigma_b = 2.30 b^2 \sqrt{\sum_{i=1}^{n} (M_i - \bar{M})^2 / n(n-1)}. \qquad (3)$$

One of the necessary conditions for calculating *b*-value is that the minimum magnitude of completeness Mc for the specific earthquake data sample selected for the study should be known. Many methods have been proposed in the literature for estimating this magnitude (Gomberg, 1991; Kijko and Sellevoll, 1992; Rydelek and Sacks, 1989; Smirnov, 1997; Wiemer and Wyss, 2000; 2002; Wiemer, 2001; Woessner and Wiemer, 2005; Papadopoulos and Baskoutas, 2009; Mignan and Woessner, 2012). At the same time, it is known that the simplest and most reliable way to estimate the Mc magnitude is to use the FMD of the earthquakes (Wiemer and Wyss, 2000; Popandopoulos and Lukk, 2014).

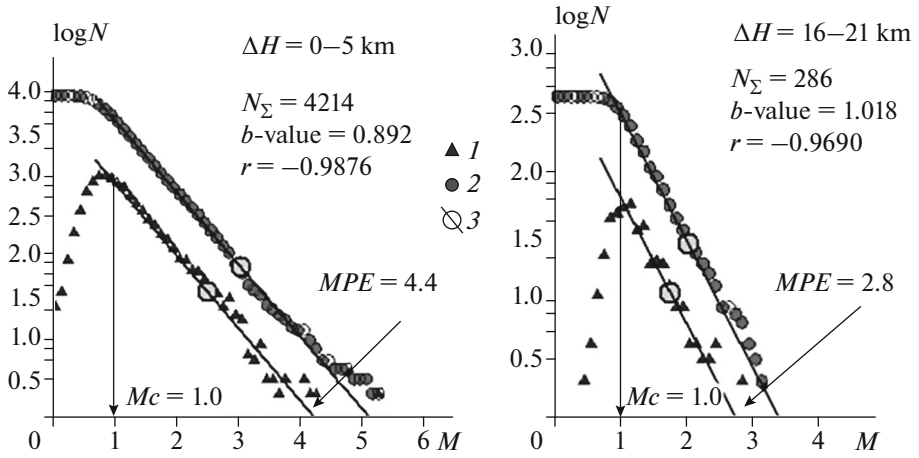

Fig. 2. Frequency-magnitude distributions (FMD) of earthquakes for two depth intervals in Kaudal LR. Determination of minimum magnitude of completeness *Mc*, Gutenberg–Richter *b*-value, and minimum magnitude of predicted earthquake (*MPE*). *1*, discrete FMD; *2*, cumulative FMD; *3*, position of midpoint M^* and $\log N^*$.

In the FastBEE program, the *Mc* value is determined by visual scanning of the magnitude on the discrete FMD of the earthquakes directly displayed on the PC's monitor and by detecting the starting point of the linear trend of the decrease in the number of earthquakes with the increase in their magnitudes (Fig. 2). As the reliability criterion of *Mc* determination, the coefficient of correlation *r* between the observed FMD and the approximating line corresponding to the GR law is used. In the previous works (Popandopoulos and Baskoutas, 2009; Lukk and Popandopoulos, 2012) it was shown that reliable *Mc* determination is achieved at the correlation coefficient $r \geq 0.95$.

The calculation accuracy of the minimum magnitude of completeness *Mc* is determined by the magnitude bin value used in the construction of FMD and is equal to half of its value. In our case, the magnitude bin is $\Delta M = 0.1$, which indicates that the *Mc* is determined accurately to ± 0.05. The detailed description of the FastBEE algorithm and the analysis of determination reliability of the *Mc* and *b*-value are presented in (Papadopoulos and Baskoutas, 2009; Lukk and Popandopoulos, 2012; Popandopulo and Lukk, 2014; Popandopoulos and Chatziioannou, 2014; Popandopoulos et al., 2016; Popandopoulos, 2018).

In order to more fully describe the results of the analysis, let us briefly outline the technique of the study. The FastBEE menu offers the options to specify the spatial characteristics of the local area (LR) of the sample, the parameters of the earthquake data, and the parameters of the filter for constructing the time series.

The LR location and size are, as a rule, determined by the a priori seismological and geotectonic features of the region. The LR can be specified by a rectangle of any size oriented in the arbitrary azimuth (Fig. 1). Depending on the objectives of the study, the LR can be oriented both along and across the strike of the seismotectonic structures (Fig. 1). The parameters of the sample of earthquake data which include the time interval *T* of the study, the magnitude range of interest $M_{\min}$ and $M_{\max}$, the interval of the source depths of the earthquakes $H_{\min}$ and $H_{\max}$, and the averaging time window *w*, are selected in such a way as to satisfy the criteria of the experiment and then stored in the information file for the subsequent use.

In addition, for each LR, the parameter determining the threshold of the minimum magnitude of the predicted earthquake (*MPE*) is specified. The *MPE* parameter indicates the *minimum* magnitude of a strong earthquake whose preparation process probably begins to manifest itself in the time series of the studied parameters. Similar to the *Mc* determination, this value is calculated based on the discrete FMD of the earthquakes constructed for the studied time interval *T*. To this end, the largest magnitude M_{larg} over the sample under study is determined. This magnitude corresponds to the intersection of the GR graph with the axis of magnitudes *M* (Fig. 2). The minimum *MPE* value is selected within $M_{\text{larg}} \approx \pm 0.3$. From the physical standpoint, the selection of the minimum *MPE* is motivated by the fact that the analysis of time variations in various prognostic parameters should rely on a predicted earthquake whose magnitude should be fairly large compared to the magnitudes of the background earthquakes. At the same time, the occurrence of the *MPE* events should be relatively rare in order that it would be possible to analyze the time variations of the studied parameters during the preparation of these events. Examining the FMD overall, we see that such earthquakes fall in the right segment of the GR graph in the region of its intersection with magnitude axis *M*. Clearly, if the sample contains one earthquake of maximum magnitude that occurred during the

studied period of time, this event will not be recorded in the FMD because $\log(1) = 0$, and only starting from two or more earthquakes, do they affect the construction of the GR graph. It is these largest magnitudes of the earthquakes that are of interest for us from the standpoint of analyzing the behavior of the time variations in *b*-value. The time interval of the study at which the *MPE* events relatively reliably appear in the *b*-value time series depends on the saturation time at which the FMD of the earthquakes is formed (from the standpoint of determination of its parameters). For the Garm region, the saturation time is 23 years. The program automatically marks the occurrences of the earthquakes with $M \geq MPE$ on the time axis of the time series.

The time series are constructed by averaging the monthly sums of ΔM (the magnitudes falling in the given magnitude bins) using a triangular filter, and then the *b*-value is calculated (Popandopoulos and Baskoutas, 2011; Popandopoulos, 2018). As known, a triangular filter is a low-pass filter that passes the signals with the periods higher than half the length of the smoothing window without distortion and is practically free of side effects (Bath, 1974). The resulting *b*-values are attributed to the end of the smoothing window. We note that the length of the smoothing window W_{month} depends on the seismic activity of the LR sample and is determined by the minimum number of the data falling in this window. We recall that the minimum number of earthquakes *N* falling into the smoothing window should be at least 50, which is one of the main conditions for estimating the uncertainty of *b*-value calculation (Marzocchi and Sandri, 2004; Sandri and Marzocchi, 2007; Woessner and Wiemer, 2005; Mignan and Woessner, 2012).

4. TIME VARIATIONS IN *b*-VALUE AS FUNCTION OF DEPTH LEVEL IN THE EARTH'S CRUST

In (Popandopoulos, 2018), the time variations in *b*-value were studied in detail in one of the seismically most active local regions (LR Kaudal) of the Garm testing area. In particular, it was shown that before most strong earthquakes with magnitudes $M \geq MPE$, characteristic anomalies exceeding one-sigma level of statistical significance were observed in the time behavior of the *b*-value. It was shown that the precursory *b*-value variation has a positive bay-like shape. The study in the cited work was based on the data for the earthquakes that occurred in the depth interval 0–16 km. At the same time, it is known that one of the remarkable properties of the GR relationship is that it contains information on the tectonic stresses in the Earth's crust directly in the area spanned by a given sample of the earthquakes (Mogi, 1962; Scholz, 1968; 2015; Main et al., 1992; Mori and Abercrombie, 1997; Wyss, et al., 2001; Schorlemmer et al., 2004a; 2004c; 2005; Spada, 2013). This factor can be used for studying the time changes in the tectonic stresses at different crustal depths. In the other words, the GR relationship provides the possibility to conduct sort of "deep sounding" of the LR zones of the sample for studying the geodynamic processes in the different depth intervals.

For performing this experiment, we studied the time variations in the *b*-value using the data for the earthquakes that occurred in the depth interval from 0 to 21 km within the same Kaudal LR (Fig. 1). As noted above, this region is located in the center of the system of seismic observations where the hypocenter location accuracy varies within ±(1–2) km, and the minimum magnitude of completeness is $Mc \approx 1.0$ (Popandopoulos, 1991; Popandopoulos and Nersesov, 1991; Popandopoulos and Lukk, 2014; Popandopoulos, 2018).

Let us illustrate the technique of this "deep sounding" by the example of two data samples of the earthquakes pertaining to the different depth intervals. Figure 2 shows the FMD of the earthquakes constructed for two depth intervals from 0 to 5 and from 16 to 21 km, respectively. The obtained FMD show that the minimum magnitude of completeness is $Mc = 1.0$ for the both horizons whereas the average *b*-values are substantially different in the upper and lower depth intervals (0.89 and 1.02, respectively). During the period under study, the total number of earthquakes (N_Σ) that occurred in the upper layer of the LR sample is 4214, whereas in the lower layer there were $N_\Sigma = 286$ events. An important fact is that the *MPE* magnitudes significantly differ in the two horizons pertaining to the same Kaudal LR: the *MPE* magnitude is 4.4 in the depth interval $\Delta H = 0$–5 km and 2.8 in the depth interval $\Delta H = 16$–21 km.

Figure 3 illustrates time variations in *b*-value for the corresponding depths. The time series were constructed with a smoothing window of 17 months moved with a step of one month. We note that when the analysis is conducted for the time series having different statistical characteristics, the length of the smoothing window should be universal (i.e., identical) for all the time series for which at least 50 earthquakes should fall in the smoothing window throughout the entire study interval (Marzocchi and Sandri, 2004). In other words, in the joint analysis of the time series, the length of the smoothing window for reducing these time series to a unified frequency content is determined based on the time series with fewest data for which the condition $N \geq 50$ is satisfied. In our case, the minimum length of the averaging window at which the requirements for obtaining statistically significant results are satisfied for all the considered time series was 17 months.

In the figure, vertical lines in the *b*-value graphs show the 70% confidence interval corresponding to the σ_b value, which is calculated at each step of data averaging by formula (3). Vertical arrows show the strong earthquakes with $M \geq MPE$ that occurred

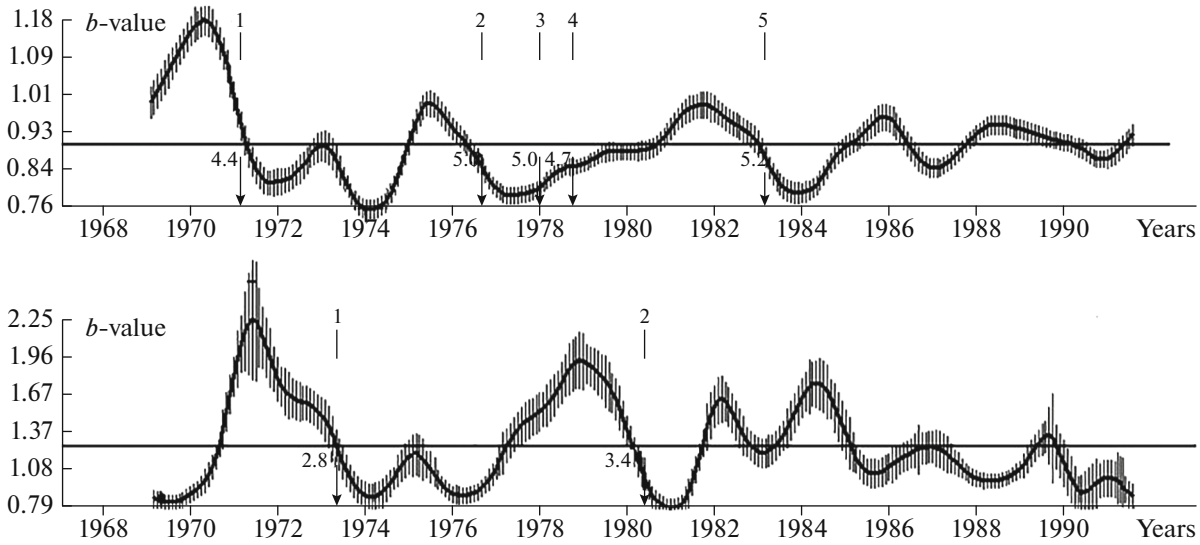

Fig. 3. Time variations in *b*-value from earthquake data in Kaudal LR (Fig. 1) for depth intervals 0–5 km (top) and 16–21 km (bottom). Arrows indicate "strong" earthquakes with magnitude $M \geq MPE$. Vertical lines in graphs mark 70% confidence interval.

within the studied horizon. Above the arrows are the numbers of earthquakes in the order of their occurrence, and below the arrows are the magnitudes of these events. It can be seen that, five earthquakes with $M \geq MPE = 4.4$ occurred during the study period in the depth interval ΔH from 0 to 5 km and only two events with $M \geq MPE = 2.8$ occurred in the depth interval ΔH from 16 to 21 km.

The curves presented in Figure 3 show that among the five events that occurred in the depth interval ΔH from 0 to 5 km, only three (nos. 1, 2, and 5) were preceded by positive bay variations in *b*-value exceeding the significance level of $2\sigma_b$. It can be seen that before earthquakes nos. 3 and 4, significant variations in *b*-value are not observed. The probable causes of this time behavior of *b*-value before the earthquakes with $M \geq MPE$ will be discussed later.

The similar *b*-value anomalies are observed in the depth interval ΔH from 16 to 21 km before earthquakes nos. 1 and 2 which, however, have the magnitudes $M = 2.8$ and $M = 3.4$, respectively. Here, the statistically significant observed variations in *b*-value in this depth interval in the period of 1982 and 1984 are not accompanied by the strong events with $M \geq MPE$. The pattern and probable causes of this behavior of the *b*-value will also be considered below. However, it is worth noting that during the 23-year study period, only two earthquakes with $M \geq 2.8$ took place in this depth interval, and these events were preceded by the most intense bay anomalies in the time behavior of *b*-value. It can be said that the earthquakes of this magnitude are almost as rare of a phenomenon for this depth as the earthquakes with $M \geq 4.4$ for the depths ΔH from 0 to 5 km where only five such events them occurred. From this it follows that the emergence of the earthquakes with $M \geq MPE = 2.8$ in the depth interval of 16–21 km is, from the standpoint of time variations in the tectonic stresses of the medium within this horizon, equally significant as the occurrence of the earthquakes with $M \geq MPE = 4.4$ in the depth interval from 0 to 5 km. We also note that a visible correlation between the curves shown in Figure 3 for two conditional horizons (0–5 and 16–21 km) is absent. This analysis illustrates the technique for studying the time changes in the *b*-value for different horizons. It is shown that the time variations in *b*-value and the FMD of the earthquakes have a different character for two depth intervals pertaining to the same LR of the sample of the earthquakes.

Extending this technique of the analysis to the entire depth range from 0 to 21 km, we have studied the time variations in *b*-value in a moving sequence of the conditional horizons with a thickness of 5 km shifted along the depth with a step of 2 km. As previously, for each conditional horizon, we constructed the FMD of the earthquakes based on which we determined the minimum magnitude of completeness *Mc*, the average *b*-value and its root mean square error σ, the minimum *MPE*, and the total number of earthquakes N_Σ (Table 1). We note that for all the conditional horizons of a given LR, the *Mc* is 1.0. The root-mean-square error σ of calculation of *b*-value presented in Table 1 for each conditional horizon testifies to the significant changes in this parameter with depth.

According to the data presented in column 2 of Table 1, in the upper horizons of the crust within the depths from $\Delta H = 0$–5 km to $\Delta H = 4$–9 km, the *b*-value varies from 0.90 to 0.94. In the deeper horizon ΔH from 10 to 15 km, the *b*-value sharply drops to 0.83

Table 1. Depth ranges ΔH of conditional horizons, average *b*-value and its variance σ, time series variability Var(%), minimum magnitude of predicted earthquake *MPE*, number N_Σ of earthquakes with $M \geq Mc$ in conditional horizon ΔH

No.	ΔH, km	$b \pm \sigma$	Var(%)	*MPE*	N_Σ
	1	2	3	4	5
1	0–5	0.906 ± 0.0086	9.5	4.4	4214
2	2–7	0.922 ± 0.0082	8.9	4.4	4936
3	4–9	0.941 ± 0.0077	8.15	4.2	4923
4	6–11	0.890 ± 0.0085	9.55	4.1	3633
5	8–13	0.878 ± 0.0125	14.2	4.1	2383
6	10–15	0.833 ± 0.0115	13.9	4.1	1559
7	12–17	1.047 ± 0.0253	24.1	3.7	851
8	14–19	1.170 ± 0.0280	23.9	3.0	464
9	16–21	1.283 ± 0.0349	27.2	2.8	286

and then again increases to 1.23 at the depths of 16 to 21 km. Similar results for the depth dependence of the time variations in the *b*-value in the discussed Kaudal LR (Fig. 5c) were obtained in our previous work (Popandopoulos and Lukk, 2014) where we studied the spatial variations of this parameter in the Garm region. The results presented in Fig. 5c are obtained by averaging the data in the depth interval of 1 km. Given the different averaging methods used in these studies, the obtained results agree quite well.

With the obtained seismicity parameters taken into account, we constructed the graphs of time variations in *b*-value for each conditional horizon (Fig. 4). In this context, it is interesting to study the variability of the *b*-value time series depending on the depth interval of the selected conditional horizons. We recall that the variability Var(%) of a time series is the ratio of the average amplitude of the fluctuations in the time series to its average value expressed in percent. According to the data presented in Table 1 it can be seen that the variability Var(%) of the time series increases with increasing depth. In the depth intervals down to 11 km, the variability of the time series varies within 8.1–9.55%, slightly increases to 14.2% in the depth intervals ΔH from 8 to 15 km, and sharply grows below a depth of 15 km reaching 24–27%.

From Table 1 it also follows that *MPE* magnitude decreases with depth. For example, $MPE = 4.4$ within the depths of the first two horizons 0–5 and 2–7 km, $MPE = 4.1$ in the deeper horizons from $\Delta H = 6$–11 to $\Delta H = 10$–15 km; and $MPE = 3.0$–2.8 at the large depths within the horizons $\Delta H = 14$–19 and 16–21 km where crustal seismicity is significantly reduced (Fig. 5b).

For comparing the time series along the depth, we need to have an idea of the statistics of the earthquakes for each conditional horizon. Figure 5b shows the distribution of the number of earthquakes with depth for the selected LR. It can be seen that most events in the studied period of time fall in the depth interval from 4 to 8 km, which is reflected in the number of events in the conditional horizons $\Delta H = 2$–7 km and $\Delta H = 4$–9 km (Table 1). The burst in the number of earthquakes at a depth of 0–1 km is probably associated with the errors in hypocenter location due to the emergence of a local minimum of the functional in the calculation of the residuals of arrival times of the waves in the near-surface layer (Popandopoulos, 1983; 1991).

Let us consider the time variations in *b*-value shown in Fig. 4. Here, an important fact is that, since the graphs of the *b*-values were constructed in the moving depth intervals, the same hypocenters of the "strong" earthquakes with $M \geq MPE$ could fall simultaneously in the overlapping depth intervals of the neighboring horizons. Therefore, these earthquakes were indicated by arrows only once only on the graphs of *b*-value time variations for which the center of thickness of the horizon (horizon's midpoint along the depth) was closest to the depth position of the hypocenter of the event. In other words, the vertical arrows in Fig. 4 indicate the time of the strong earthquakes with $M \geq MPE$ whose hypocenters were located in the vicinity of the midpoint of the depth interval occupied by the corresponding conditional horizon.

Figure 5a shows a schematic vertical cross section of the LR for the discussed sample of the earthquakes. The hypocenters of the "strong" events corresponding to *MPE* for each depth interval are indicated by circles. However, due to the fact that *MPE* decreases with depth according to the data presented in Table 1, the absolute magnitude of a "strong" earthquake, in our understanding of this word, also decreases with depth remaining at the same time equally significant within its horizon. For example, in Fig. 4, in the depth interval ΔH from 0 to 5 km, all earthquakes with $M \geq MPE = 4.4$ are shown; indicated in the depth interval ΔH from 6 to 11 km are all earthquakes with $M \geq MPE = 4.1$ are shown; in the depth interval ΔH from 14 to 19 km, the events with $M \geq MPE = 3.0$ are presented, etc. (Fig. 5a, Table 1). From this it follows that the earthquakes with magnitudes $4.1 \leq M \leq 4.3$ that occur in the depth inter-

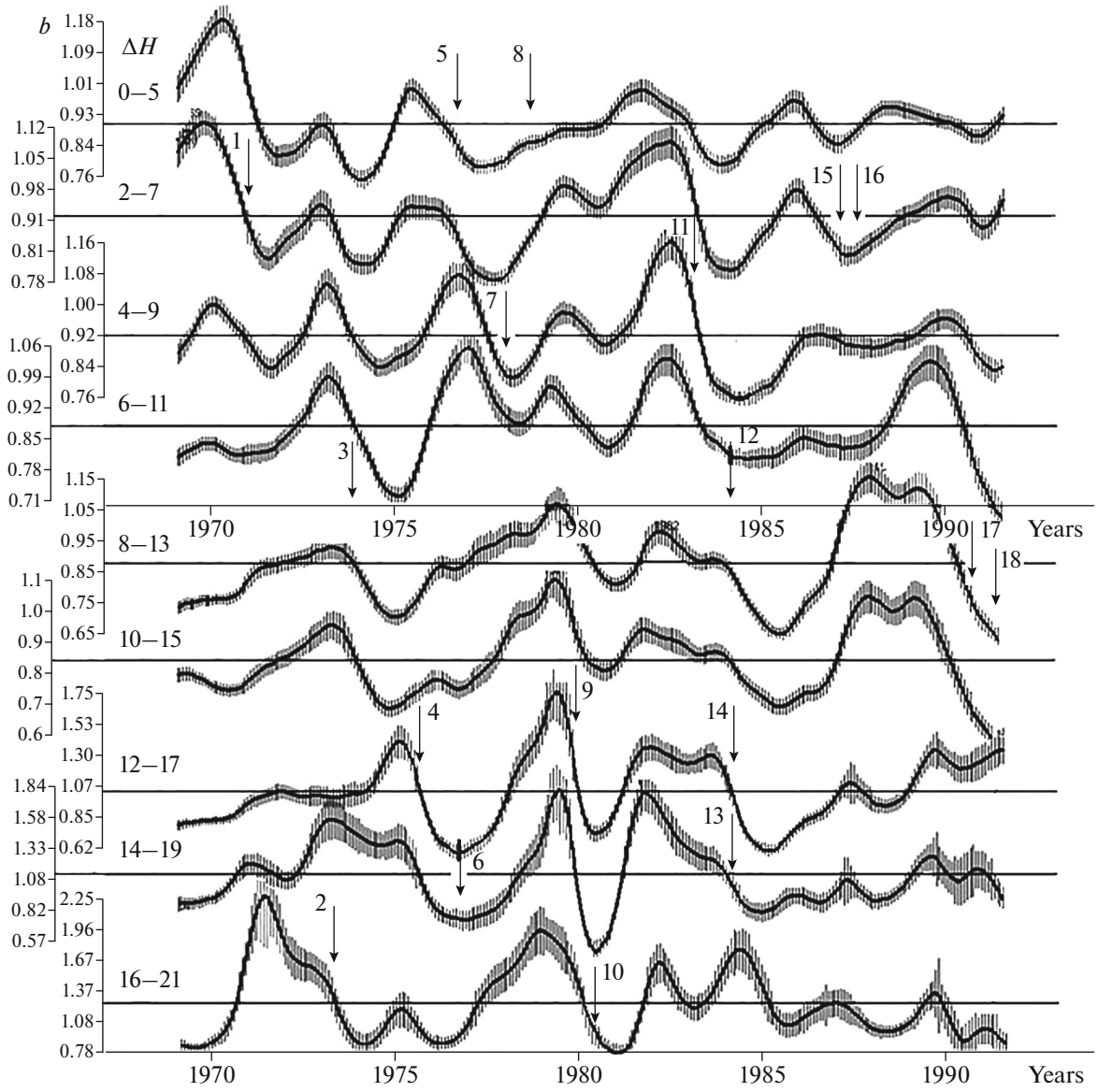

Fig. 4. Time variations in *b*-value in different depth intervals from earthquake data in Kaudal LR (Fig. 1). Vertical arrows indicate "strong" earthquakes with magnitudes $M \geq MPE$. Numbers at arrows correspond to earthquake numbers in Table 1 and Fig. 5a. Vertical lines in graphs mark 70% confidence interval.

val ΔH from 0 to 5 km are not considered "strong" because, by definition, this magnitude range for this horizon is below the minimum *MPE*. In the other words, it is possible that the earthquakes in the magnitude range $4.1 \leq M \leq 4.3$ are not indicated as strong events for the depth interval from 0 to 5 km but such events are considered strong for the depths ΔH from 6 to 11 km.

The analysis using the described procedure revealed 18 earthquakes with $M \geq MPE$ for all the conditional horizons. The catalog of these events in chronological order is presented in Table 2. In Fig. 5a, the numbers in the circles correspond to the numbers in the catalog (Table 2) and to the numbers of the arrows in Fig. 4. The size of the circle conditionally shows the relative magnitude of the "strong" event.

The analysis of the graphs in Fig. 4 shows that the time variations in *b*-value are not coherent along the depth, i.e. synchronous time changes in *b*-value are not observed in the depth range from 0 to 21 km. At the same time, it can be seen that during some periods of time, synchronous variations of the same type with the amplitudes exceeding the significance level (1σ) capture several neighboring horizons. Moreover, these anomalies are present in the overall depth interval that is larger than the selected thickness 5 km of one conditional horizon, which means that the emergence of these anomalies is not an occasional event because it

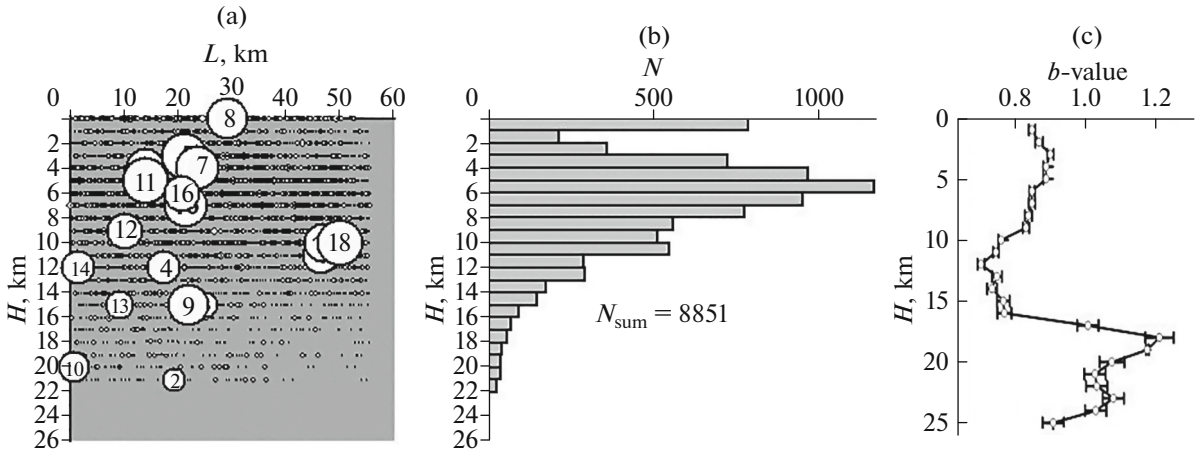

Fig. 5. Depth distribution of seismic parameters for Kaudal LR (Fig. 1): (a) hypocenters of earthquakes with $M \geq MPE$ for moving depth intervals $\Delta H = 5$ km. Circles with numbers correspond to earthquake numbers shown in Table 2; (b) distribution of numbers N of earthquakes; (c) b-values depending on depth in Kaudal LR (Popandopulo and Lukk, 2014).

reflects at least two independent realizations of data samples. For example, before the earthquake no. 1 with magnitude $M = 4.4$ and source depth $H = 4$ km (the hypocenter in Fig. 5a is overlapped by the foreground hypocenters), an anomaly is observed in the depth intervals from 0–5 to 4–9 km with the highest amplitude localized within the upper two horizons close to the hypocentral depth of this event. At the same time, this anomaly disappears at the depths of 6–11 km and below. Before earthquake no. 2 with $M = 2.8$ and $H = 21$ km (Fig. 5a), a significant anomaly is only observed in the depth interval ΔH from 16 to 21 km. The anomaly before earthquake no. 3 with $M = 4.1$ and $H = 11$ km is clearly seen at the depths of 4–9

Table 2. Catalog of earthquakes with $M \geq MPE$ in different depth intervals in Kaudal LR from 1970 to 1992

No.	Date	Lat., North	Long., East	Depth, km	Magnitude
1	2	3	4	5	6
1	Feb. 10, 1971	38.878	70.526	4	4.4
2	Apr. 23, 1973	38.934	70.571	21	2.8
3	Nov. 13, 1973	39.031	70.861	11	4.1
4	Aug. 13, 1975	38.963	70.540	12	3.7
5	Sept. 3, 1976	38.950	70.590	3	5.2
6	Sept. 30, 1976	38.974	70.627	15	3.0
7	Dec. 25, 1977	38.966	70.613	4	5.0
8	Sept. 26, 1978	38.973	70.674	0	4.7
9	Oct. 20, 1979	38.934	70.602	15	4.6
10	May 19, 1980	38.914	70.357	20	3.4
11	Feb. 26, 1983	38.937	70.508	5	5.2
12	Feb. 19, 1984	38.943	70.459	9	4.1
13	Feb. 21, 1984	38.886	70.468	15	3.4
14	Mar. 12, 1984	38.877	70.379	12	3.9
15	Feb. 23, 1987	38.968	70.585	7	4.9
16	July 17, 1987	38.955	70.582	6	4.1
17	Sept. 30, 1990	38.948	70.895	10	4.5
18	Apr. 26, 1991	39.003	70.913	10	5.2

and 6–11 km; however, the anomaly with a characteristic shape, albeit not so significant, is also distinguished at the depths of 0–5 and 10–15 km.

The anomaly that precedes earthquake no. 4 with $M = 3.7$ with $H = 12$ km is visible at a depth of 12–17 and 14–19 km. Interestingly, the anomaly before earthquake no. 5 with $M = 5.2$ and $H = 3$ km is only present in the b-value graph for the depth interval 0–5 km. At the same time, the characteristic precursory bay-like variation in the b-value behavior before the earthquake no. 8 with $M = 4.7$ and $H = 0$ km is absent. The absence of the anomaly in this case is probably associated with the location of the preparation zone of the source of a strong earthquake which is most likely to be in the near-surface layer. Earthquake no. 7 with $M = 5.0$ and $H = 4$ km is preceded by the anomalies that are clearly manifest in the depth intervals of 4–9 and 7–11 km. The characteristic positive anomalies in the b-value are present before earthquake no. 9 with $M = 4.6$ and $H = 15$ km where the highest amplitudes of the statistically significant anomalies are observed in the graphs for the depth intervals ΔH from 8–13 km to $\Delta H = 16$–21 km. At the same time, the characteristic features of the curves are preserved up to the upper horizon $\Delta H = 2$–7 km.

The similar pattern of time variations in b-value is also observed before all the other earthquakes with $M \geq MPE$. However, there is yet another remarkable characteristic example which is observed in the case of the earthquakes nos. 17 and 18 with $M = 4.5$ and 5.2, respectively, which occurred at a depth of 10 km. The clearly pronounced anomalies before these events are only present in the curves constructed in the depth interval 6–11, 8–13, and 10–15 km, respectively, i.e. for the depths in the close vicinity of the hypocentral depths of these strong events. Meanwhile, in the upper and lower horizons (0–7 and 14–21 km, respectively), the anomaly that is observed in the intermediate horizons before earthquakes nos. 17 and 18 disappears.

According to our analysis, the time behavior of b-value for different depth intervals indicates that most of the 18 earthquakes with $M \geq MPE$ in the Kaudal LR are preceded by significant anomalies in the form of positive bays, which are localized in the vicinity of the sources of these events. Moreover, the maximum amplitudes of these anomalies are concentrated close to the hypocenters of the strong earthquakes and decay with distance from the source.

The picture presented in Fig. 4 helps us to explain the absence of the anomalies in the time behavior of b-value before earthquakes nos. 3 and 4 in the depth interval ΔH from 0 to 5 km considered above in Fig. 3. (We note that earthquakes nos. 3 and 4 in Fig. 3 correspond to earthquakes nos. 7 and 8 in Fig. 4 and Table 2.) It can be seen that the precursory anomaly before earthquake no. 3 (Fig. 3) is absent in the depth interval of 0–5 km; however, a clearly pronounced anomaly is seen at the depths of 4–11 km (Fig. 4). From this it follows that the probable process of the preparation of earthquake no. 7 does not capture the near-surface layer in the depth interval from 0 to 5 km (earthquake no. 3 in Fig. 3) but is localized at the depths of 4–11 km.

At the same time, the fact that all the curves in 1972–1984 are correlated (with a certain phase shift in 1975–1978 in the lower horizons from 4 to 11 km) allows us to interpret the overall pattern of the time variations in b-value before earthquakes nos. 5 and 7 (Fig. 4) as reflecting a single process of the changes in the tectonic stresses in the depth interval from 0 to 11 km. In this case, earthquakes nos. 5 and 7 can be considered as paired events at which after the first earthquake no. 5, the stresses in the upper horizon were dissipated whereas in the lower horizons they were preserved forming the condition for the emergence of earthquake no. 7. At the same time, the absence of the anomaly before earthquake no. 4 in Fig. 3 (i.e., no. 8 in Fig. 4) can probably be associated with the preparation of this event in the near-surface zone because the hypocentral depth of this event is 0 km. The absence of the earthquakes before the observed anomalies of 1982 and 1984 in the curves of Figure 3 in the depth interval from 16 to 21 km can be associated with the occurrence of the strong earthquakes nos. 13 and 14 (Fig. 4) whose sources had the hypocenters at the depths of 12 and 15 km.

Thus, our analysis suggests that the differentiation of the time variations in the b-value along the depth confidently reveals positive bay-like anomalies before the earthquakes with magnitudes $M \geq MPE$. One of the important conclusions is that in the vast majority of cases, the highest amplitudes of the b-value anomaly before the strong earthquakes with $M \geq MPE$ are observed in the depth intervals close to the depths of the preparation of the sources of these events. As a result, based on the conducted study, we may state that the differentiation of the time variations in b-value along the depth will allow us to estimate the depths of impending strong earthquakes.

5. TIME VARIATIONS IN b-VALUE ALONG LATERAL STRIKE OF THE EARTH'S CRUST

One of the purposes of this work is to study the time variations in b-value depending on the lateral position of the LR of the sample. This analysis is interesting from the standpoint of revealing the general regularities in the b-value time variations before the "strong" earthquakes with $M \geq MPE$ whose FMD characteristics are spatially different. Another important feature of this analysis is that it can help detecting the probable deformation fronts in the Earth's crust caused by the migration of the sources of the weak earthquakes (Kasakhara, 1985; Turcotte and Schubert, 1985; Bykov, 2005; Sherman, 2013). For solving this problem, we selected seven LRs along and approximately across the strike of the geotectonic structures located

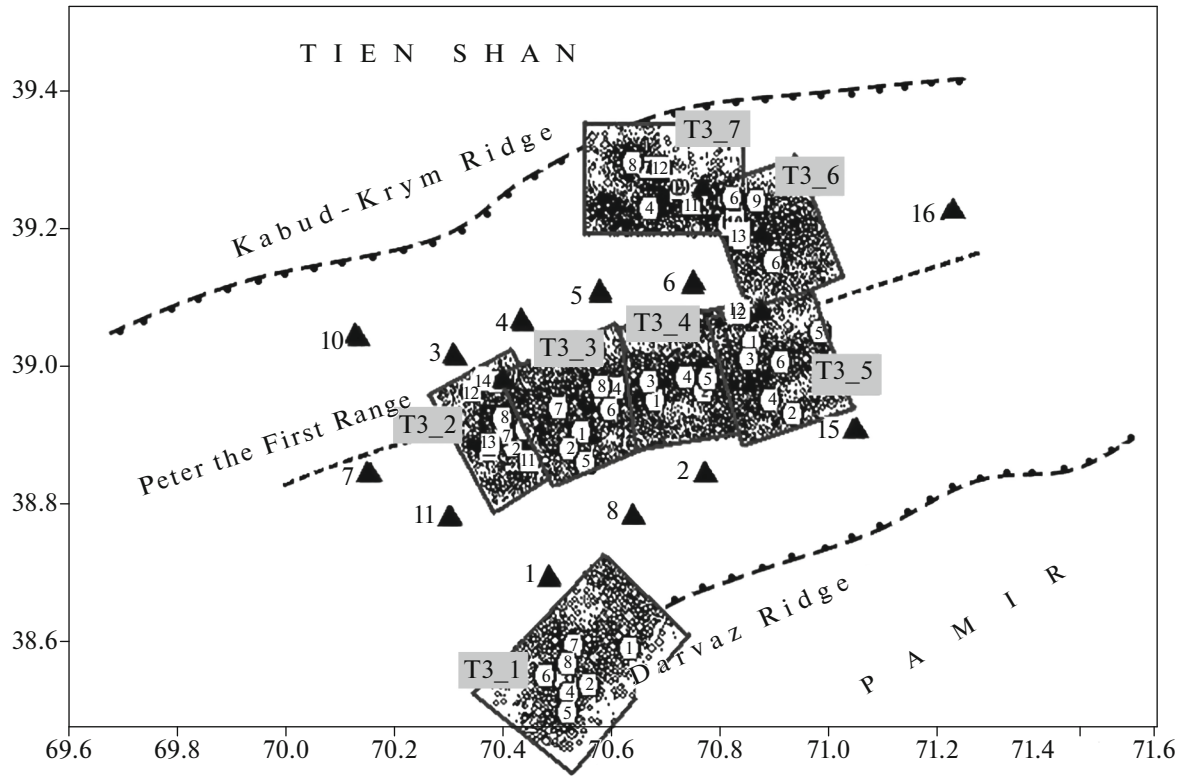

Fig. 6. Schematic layout of earthquake data sample's local regions (LRs) located along lateral strike of geotectonic structures. Designations are indicated in Fig. 1. Open circles with numbers are earthquakes' epicenters with $M \geq MPE$ within LR.

in the regions with relatively high seismicity of the observation region (Fig. 6).

Figure 7a illustrate the time variations in *b*-value calculated from the data on the weak earthquakes that occurred in the T3_2, T3_3, T3_4, and T3_5 LRs (Fig. 6) located along the strike of the main geotectonic structures aligned with the Peter the First Range. Figure 7b shows the *b*-value variations according to data from the T3_1, T3_3, T3_6 and T3_7 LRs (Fig. 6) located practically across the strike of the above structures. The analysis was conducted for the events that occurred in the depth interval from 0 to 30 km. The parameters of the filter of the time series were the same as in the previous Section.

Initially, for each LR of the sample, the FMDs of the earthquakes were constructed, and the parameters of seismicity were determined (the average *b*-value and its root mean square scatter σ, the minimum magnitude of completeness *Mc*, the minimum magnitude of predicted earthquake *MPE*, and the number N_Σ of the earthquakes used in the analysis) (Table 3). The data presented in Table 3 show that the average *b*-value for each LR of the sample is different and varies from 0.882 ± 0.0101 to 1.121 ± 0.017. This corresponds to the spatial heterogeneity of the *b*-value in the Garm region which has been studied in detail and presented in (Popandopulo and Lukk, 2014). The *Mc* value, as is known, depends on the LR's location relative to the observation system and varies from 1.0 to 1.4 (Lukk and Popandopulo, 2012). An important fact is that the minimum magnitude of the predicted earthquake (*MPE*) is individual for each LR of the sample and varies from 3.3 to 4.3. The number N_Σ of the earthquakes with magnitude of at least *Mc* that occurred between 1967 and 1991 in each LR varies from 894 to 3313. It can be seen that the variability Var(%) of the time series is also different in spatial terms and varies from 7.65 to 18.78%. However, in contrast to the distribution of this quantity along the depth, no apparent regularity is observed in its relation with geotectonics or with other parameters—the average *b*-value, *Mc*, *MPE*, and N_{earthq}. We note that in most of the LRs of the sample, more than one hundred earthquakes fall in the selected averaging window (17 months). The T3_6 LR is the exception: here, the average number of earthquakes in the averaging window varies about 50. We recall that this number of the events is sufficient for ensuring statistically reliable estimation of *b*-value in the selected averaging window (Marzocchi and Sandri, 2003).

Vertical arrows in Figs. 7a and 7b mark the time of the earthquakes with magnitudes $M \geq MPE$ for each LR of the sample. In the upper part of each curve, the sequence number *N* of each "strong" event is indicated, and the magnitudes *M* of these events are indicated on the corresponding time axis in the lower part

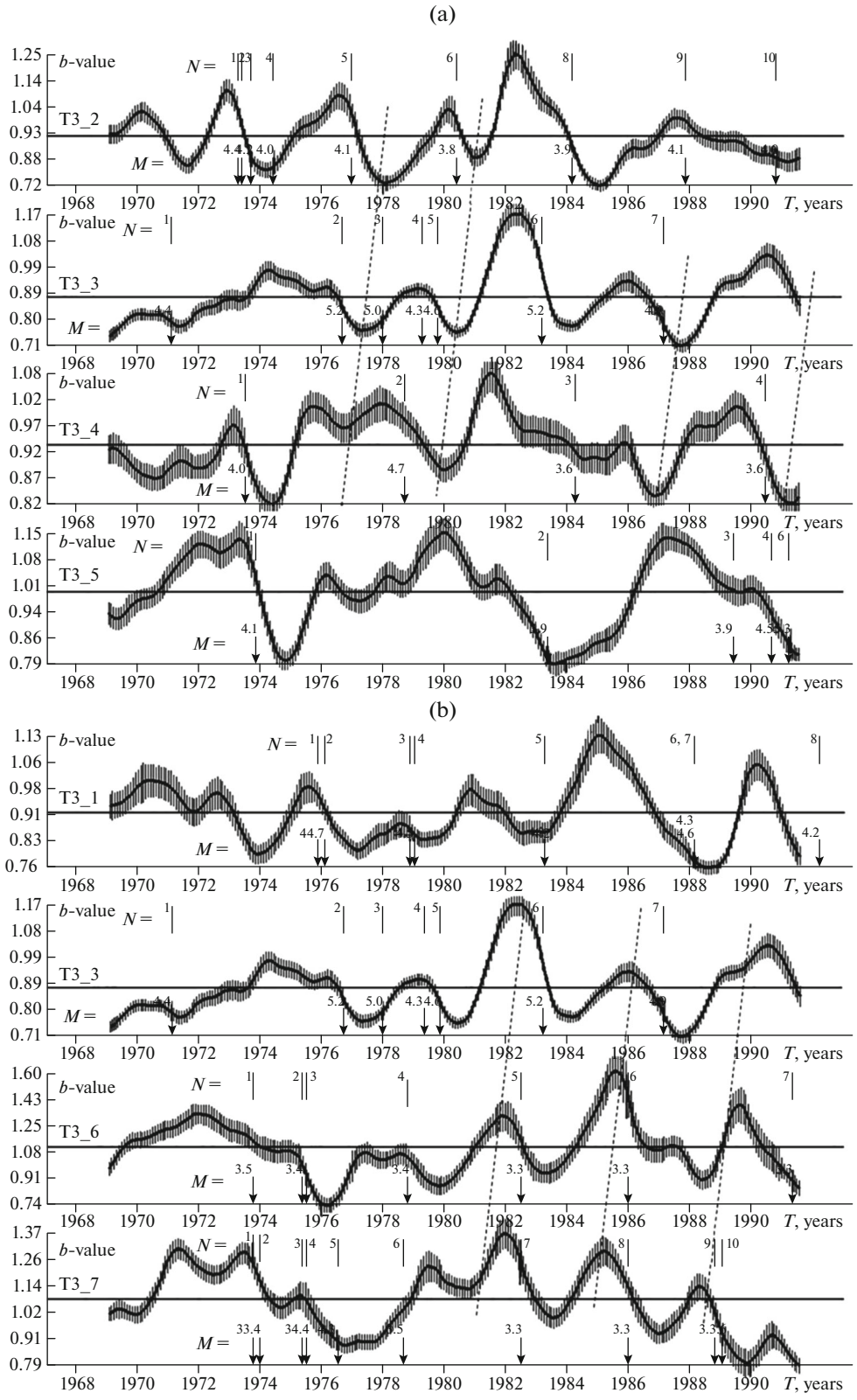

Fig. 7. (a) Time variations in *b*-value based on earthquake data in LRs (Fig. 6) located along strike of geotectonic structures. Vertical arrows mark earthquakes with magnitudes $M \geq MPE$ within each LR. Numbers at arrows correspond to earthquakes' numbers indicated in Table 4. Vertical lines in graphs mark 70% confidence interval. Dashed lines indicate probable signs of propagation of deformation wave front; (b) time variations in *b*-value based on earthquakes in LRs (Fig. 6) located across strike of geotectonic structures. Designations are same as in Fig. 7a.

Table 3. Characteristics of *b*-value time series depending on lateral strike of local region of earthquake sample

No.	LR	$b \pm \sigma$	Var(%)	*Mc*	*MPE*	N_Σ
1	T3_1	0.919 ± 0.0087	10.94	1.4	4.2	2020
2	T3_2	0.918 ± 0.0113	15.08	1.1	3.8	1769
3	T3_3	0.882 ± 0.0101	13.22	1.1	4.3	3313
4	T3_4	0.937 ± 0.0060	7.65	1.0	3.6	3162
5	T3_5	0.994 ± 0.0102	11.59	1.0	3.9	2886
6	T3_6	1.121 ± 0.0170	18.78	1.2	3.3	894
7	T3_7	1.086 ± 0.0148	15.16	1.1	3.3	1705

LR is code of local region, *b* and σ are average *b*-value and its variance, Var(%), is time series variability, *Mc* is minimum magnitude of completeness, *MPE* is minimum magnitude of predicted earthquake, N_Σ is number of earthquakes with $M \geq Mc$ in LR.

of the curves. The catalog of the "strong" earthquakes for each LR of the sample is presented in Table 4. The numbers in Table 4 (*N*) correspond to the numbers *N* shown in Figs. 7a and 7b.

The behavior of the *b*-value curves calculated for the LRs aligned with the strike of the Peter the First Range (Fig. 7a and Fig. 6) show that in the vast majority of the cases, anomalous positive bay-like variations in the *b*-value are observed before the "strong" events with $M \geq MPE$. We note that, as previously (Popandopulo, 2018), a single "strong" event is understood here as a group of the earthquakes that are spaced in time by less than the length of the averaging window.

For example, the T3_2 LR with $M \geq (MPE = 3.8)$ was struck by ten strong events (Table 4). Among these earthquakes, a group of the events *N*1–*N*4 was preceded by a significant biennial anomaly. A similar situation is observed before each of the events *N*5, *N*6, *N*7, *N*8 and *N*9. The anomaly before the *N*10 earthquake is absent; however, in the neighboring region T3_3 LR, this event is preceded by a significant anomaly which is most likely to be related to this earthquake. And vice versa, the anomaly observed in 1969–1970 is not accompanied by a strong event. This anomaly most probably marks the preparation of the strong event *N*1 with $M = 4.4$ which took place in the neighboring T3_3 LR. As a result, during the 20-year observation period, among seven "strong" events with $M \geq MPE$ that occurred in the T3_2 LR, five events were successfully forecast, one event was missed, and one anomaly was false. Moreover, the missed earthquake *N*10 and the false anomaly of 1969–1970 can be accounted for by the processes taking place in the neighboring LR.

In T3_3 LR, six "strong" events with $M \geq (MPE = 4.3)$ occurred. Earthquake *N*1 is not preceded by an anomaly; however, as mentioned above, the anomaly in the neighboring LR T3_2 of 1969–1970 can be considered as a sign of the preparation of this event. Before the earthquake *N*2, with $M = 5.2$, a characteristic biennial *b-value* change is observed. Earthquakes *N*3 and *N*4, *N*5 are not preceded by characteristic variations *b*. Before the earthquake *N*6 with $M = 5.2$, a natural two-year anomaly is observed. And finally, before the earthquake *N*7 with $M = 4.9$, a small anomaly can be distinguished. The end of the anomaly of 1990–1991. it is not accompanied by an earthquake with $M \geq MPE$; at the same time, event *N*6 with $M = 5.3$ (Table 4) occurred in the neighboring T3_5 LR, the preparation zone of which could also cover the T3_3 LR zone. In general, it can be said that for 6 "strong" events with $M \geq 4.3$ that occurred in this LR, one can predict with confidence 3 events, three events are not preceded by anomalies and one anomaly is false, after which a strong event does not occur.

The analysis of the time variations for the T3_4 LR shows that during the study period, four strong events $M \geq (MPE = 3.6)$ occurred in this region, and each of these events was preceded by a characteristic bay-like anomaly in the *b*-value. The same also applies for T3_5 LR where the minimum *MPE* is 3.9. Here, similar anomalies lasting up to three years are observed before three strong events. However, against the background decrease in the *b*-value curve in 1987–1990, two "strong" events *N*3 and *N*4, 5, 6 took place.

Let us now consider the *b*-value curves calculated for the LRs oriented across the strike of the geological structures (Fig. 7b). The T3_1 LR was struck by five events with $M \geq MPE$ (Table 4). It can be seen that four of them are preceded by distinct anomalies; before one event *N*3,4 significant changes in the *b*-value are absent, and two false anomalies are observed in the period 1970–1971. The *b*-value curve of the T3_3 LR was considered above and is presented here for convenient analysis of the profile across the strike of the geological structures. Among the six "strong" earthquakes in the T3_6 LR, four events had the clear precursory anomalies and two events (*N*2, *N*3 and *N*4) occurred without any significant changes in the *b*-value. Finally, 7 "strong" events occurred in T3_7 LR; four of them (*N*1, *N*2, *N*7, *N*8 and *N*9, *N*10) are preceded by the significant anomalies in the *b*-value, and three events *N*3, *N*4, *N*5 and *N*6 are not accompanied by the marked anomalies.

Table 4. Catalog of earthquakes with $M \geq MPE$ in LRs located along and across strike of geological structures from 1967 to 1992

No.	Date	Lat., North	Long., East	Depth, km	Magnitude
1	2	3	4	5	6
	T3_1				
1	Nov. 2, 1975	38.596	70.635	4	4.2
2	Jan. 23, 1976	38.542	70.560	0	4.7
3	Nov. 17, 1978	38.552	70.513	3	5.0
4	Dec. 30, 1978	38.531	70.524	2	4.5
5	Apr. 4, 1983	38.503	70.520	4	4.2
6	Feb. 18, 1988	38.556	70.479	5	4.3
7	Feb. 20, 1988	38.599	70.532	7	4.6
8	Mar. 15, 1992	38.573	70.522	5	4.2
	T3_2				
1	Apr. 21, 1973	38.886	70.429	3	4.1
2	May 21, 1973	38.884	70.424	3	4.0
3	Sept. 13, 1973	38.906	70.447	0	4.2
4	June 13, 1974	38.882	70.478	11	4.0
5	Dec. 19, 1976	38.973	70.393	8	4.1
6	May 19, 1980	38.921	70.404	8	3.8
7	Feb. 19, 1984	38.943	70.459	9	4.1
8	Mar. 12, 1984	38.877	70.379	12	3.9
9	July 10, 1985	38.862	70.455	9	4.1
10	Nov. 4, 1990	38.885	70.382	5	4.0
	T3_3				
1	Feb. 10, 1971	38.878	70.526	4	4.4
2	Sept. 3, 1976	38.950	70.590	3	5.2
3	Dec. 25, 1977	38.966	70.613	4	5.0
4	Apr. 16, 1979	38.860	70.556	6	4.3
5	Oct. 20, 1979	38.934	70.602	15	4.6
6	Feb. 26, 1983	38.937	70.508	5	5.2
7	Feb. 23, 1987	38.968	70.585	7	4.9
	T3_4				
1	July 26, 1973	38.960	70.772	5	4.1
2	Sept. 26, 1978	38.973	70.674	0	4.7
3	Apr. 12, 1984	38.980	70.739	7	3.6
4	July 1, 1990	38.979	70.780	5	3.6
	T3_5				
1	Nov. 13, 1973	39.031	70.861	11	4.1
2	May 26, 1983	38.929	70.934	7	3.9
3	June 7, 1989	39.007	70.856	10	3.9
4	Sept. 30, 1990	38.948	70.895	10	4.5
5	Mar. 30, 1991	39.045	70.987	3	4.1
6	Apr. 26, 1991	39.003	70.913	10	5.3

Table 4. (Contd.)

No.	Date	Lat., North	Long., East	Depth, km	Magnitude
1	2	3	4	5	6
	T3_6				
1	Oct. 3, 1973	39.215	70.828	7	3.5
2	May 20, 1975	39.213	70.832	10	3.3
3	July 2, 1975	39.237	70.829	9	4.4
4	Oct. 21, 1978	39.146	70.901	9	3.4
5	July 2, 1982	39.198	70.820	9	3.3
6	Dec. 28, 1985	39.201	70.832	9	3.3
7	May 14, 1991	39.232	70.873	6	3.3
	T3_7				
1	Oct. 3, 1973	39.215	70.828	7	3.5
2	Dec. 24, 1973	39.220	70.676	9	3.4
3	May 20, 1975	39.213	70.832	10	3.3
4	July 2, 1975	39.237	70.829	9	4.4
5	July 10, 1976	39.279	70.670	5	4.8
6	Sept. 5, 1978	39.286	70.645	6	3.5
7	July 2, 1982	39.198	70.820	9	3.3
8	Dec. 28, 1985	39.201	70.832	9	3.3
9	Oct. 23, 1988	39.227	70.754	6	3.3
10	Jan. 30, 1989	39.280	70.698	10	3.6

Above, we examined the emergence of the anomalous period with a positive bay-like variation before the earthquakes with magnitudes $M \geq MPE$ in the LRs within the observation region. Since the timespan of our analysis is relatively large (it covers 23 years and includes quite a few anomalous periods accommodating 38 "strong" events with magnitudes $M \geq MPE$), we may try to estimate the quality of the medium-term earthquake forecast using the FastBee algorithm (Papadopoulos and Baskoutas, 2009). For doing this, we use the well-known formulas for the reliability of the alarms of anomalous periods (p_1) and the total (overall) reliability of the forecast of the strong earthquakes (p_2) proposed in (Kasahara, 1981):

$$p_1 = m/F, \quad p_2 = m/M, \tag{4}$$

where $F = M + n$ and $M = M + \mu$ are the total number of the alarm messages and the total number of the occurred events, respectively. Here, m is the number of the true (successful) forecasts, n is the number of false alarms, and μ is the number of missed events. The values of these parameters for each LR separately and their total number are presented in Table 5. From the presented data it follows that the alarm reliability is $p_1 = 0.844$ and the overall reliability of the forecast is $p_2 = 0.71$. Hence, in 84% of cases, the emergence of the observed *b*-value anomalies in the LR ends in the occurrence of the strong earthquakes with $M \geq MPE$ whereas the average probability of successful forecasting of the event is 71%.

At the same time, it should be born in mind that, based on the conclusions made in the previous section, i.e. in the case of differentiated monitoring of time variations in *b*-value at different depths, the prognostic estimates can be significantly improved. Besides, a better forecasting quality can be achieved by joint consideration of the time variations in *b*-value calculated from the earthquake data from the neighboring LRs of the sample.

Let us now consider the probable manifestations of the deformation waves in the Earth's crust caused by the migration of the sources of weak earthquakes. Visual examination of the time variations in the *b*-value in Figs. 7a and 7b shows that, generally, the correlation between the curves obtained in the neighboring LRs is not observed. However, it can be seen that that on some intervals, there is a remarkable similarity between the shapes of *b*-value anomalies in the neighboring LRs. For example, the curves for the T3_2, T3_3, and T3_4 LRs which are located along the Peter the First Range (Fig. 6) have a fairly good visual correlation during the period from 1977 to 1984; the curves for the T3_3 and T3_4 LRs are closely correlated between 1986 to 1991. In the selected time peri-

Table 5. Alarm (p_1) and reliability (p_2) parameters for estimates of occurrence of earthquakes with $M \geq MPE$ for different LRs

LR	*m*	*n*	μ
T3_1	4	2	1
T3_2	5	1	2
T3_3	3	1	3
T3_4	4	0	0
T3_5	3	0	1
T3_6	4	0	1
T3_7	4	1	3
Σ =	27	5	11

M is number of correct (successful) forecasts, *n* is number of false alarms and μ is number of missed events.

ods, there is also a certain evident time shift between the anomalies so that the characteristic forms of the variation initially emerge in T3_4 LR and then propagate towards T3_2 LR (Fig. 6), i.e., the so-called deformation front propagating from NE to SW along the Peter th First Range is observed (Kasahara, 1985; Turcotte and Schubert 1985; Nikolaev, 1996; Bykov, 2005; Sherman, 2013). However, we cannot but note a singular type of the time variations in the curve obtained from the T3_5 LR data, where no correlation with the other curves is observed. One of the probable explanations of this behavior can be proposed based on the early studies conducted in this region relying on the data of time variations in seismic velocities (Nersesov and Popandopulo, 1988). According to this work, the boundary between the T3_4 and T3_5 LRs coincides with the boundary separating the different types of time variations in seismic velocities. This coincidence of the results of two studies that use fundamentally different seismological parameters may indicate the presence of the boundary of two structural blocks of the Earth's crust of the Garm region between the T3_4 and T3_5 LRs. In this case, we may hypothesize that the synergy of the structural blocks at their contact results in energy dissipation leading to the change in the type of tectonic deformations at the passage of the fronts of deformation waves through the boundaries of these blocks.

The apparent cross-correlation between the curves on some time intervals can also be observed in the data for T3_3, T3_6 and T3_7 LRs (Fig. 7b). Here, there is also a phase shift between the curves in the time interval 1979 to 1991. Interestingly, in this case again the probable front of the deformation wave propagates from NE to SW. Based on the existing data, i.e., the coordinates of the centers of the LRs and the time marks tracking the movement of the slow fronts (Figs. 7a, 7b), we can determine the propagation velocity of the hypothesized fronts. According to the estimates made in this way, the slow deformation waves propagate at a rate of 40–50 km/yr, which is fairly consistent with both the theoretical data and the existing field observations (Kasahara, 1985; Turcotte and Schubert, 1985; Nikolaev, 1996; Bykov, 2005). A more detailed analysis of the detection of the slow deformation waves is beyond the scope of this work; however, the approach used in this work seems promising for these studies.

6. DISCUSSION

The detailed study of the *b*-value spatiotemporal variations shows that an anomaly of a regular characteristic shape appears in this parameter before "strong" earthquakes with $M \geq MPE$. In our case, "strong" earthquakes are understood as all the earthquakes that occurred in a local region (LR) or in a conditional depth horizon if the sample of the earthquakes whose magnitudes exceed the minimum magnitude of the predicted earthquake (*MPE*). The *MPE* value is typically determined at the intersection of the line of the GR relationship with the magnitude axis. Determination of these magnitudes requires a relatively long time interval of observations (saturation time for the reliable construction of FMD of the earthquakes) on the order of dozens of years (in our case, 23 years).

It is known that seismicity is extremely spatially heterogeneous. The seismic process mainly reflects the structural heterogeneity of the medium and exposes the characteristic properties of the hierarchical system in the distribution of earthquakes in space, in time and in energy (Sadovskii and Pisarenko, 1991). From the physical standpoint, the processes taking place in each structural block have a property of self-similarity. Therefore, a structural block (LR) possessing its own geotectonic properties is characterized, inter alia, by the individual frequency-magnitude distribution (FMD) of earthquakes; besides, under time variations in the tectonic stresses, the hierarchical self-similarity of the block manifests itself, which determines the individual minimum *MPE* in each structural block. Thus, the results of spatial mapping of the minimum *MPE* again indicate that the geodynamic processes in the Earth's crust are hierarchically self-similar in a wide range of magnitudes, which is clearly seen from the data presented in Figs. 4 and 7 and in Tables 1 and 3.

The main pattern of the GR *b*-value precursor of a "strong" earthquake has a form of a positive semi-sinusoidal bay-like variation. The physics of this behavior of *b*-value can be explained based on the phenomenological model described in (Popandopulo and Baskoutas, 2011; Popandopulo, 2018). This model fits well within the "hard inclusion" model or consolidation model (Kasahara, 1981; Dobrovolsky, 1983; 1991; Ruff; 1992) and the classical model of the preparation of tectonic earthquakes known as the avalanche-unstable fracture formation model (AUF)

(Kostrov and Das, 1988; Myachkin et al., 1975; Sobolev, 1993).

The curves shown in Fig. 7a and 7b with a probability above 71% indicate that the earthquakes with $M \geq MPE$ occur in the second phase of the anomaly during the decrease in the *b*-values which is in turn preceded by a period of increase. This probability of the medium-term seismic hazard assessment is ensured by the high statistics in the analysis of 38 earthquakes with magnitudes $M \geq MPE$. At the same time, if a positive bay-like anomaly is detected in the graphs of time variations of the *b*-value, the probability of a "strong" earthquake reaches 84%.

Another important point is that the "strong" earthquakes barely occur in the first phase of this process, i.e. during the increase in the *b*-value. Examining all the curves shown in Figs. 4, 7a, and 7b, we can see that the "arrows" indicating the occurrence of a "strong" earthquake with $M \geq MPE$ are absent during the increase in the *b*-value. This regularity, in turn, can be used for medium-term of seismic hazard assessment as a period of quiescence or unlikely occurrence of a strong event (Popandopulo and Baskoutas, 2011; Popandopulo, 2018).

The time variations in *b*-value obtained from the realizations of the events in the different depth intervals are particularly interesting (Fig. 4). A careful examination of the behavior of *b*-value variations shown in Fig. 4 reveals relative similarity of the curves localized in certain horizons. All the curves clearly fall into three groups. The first (upper) group includes the first 4 curves in the depth intervals ΔH from 0–5 to 6–11 km. The second (middle) group includes the curves corresponding to the depth intervals ΔH of 8–13 and 10–15 km, and the third group comprises the curves for the depths below 12–17 km. It is remarkable that approximately the same division of the Earth's crust in this region into three horizons can also be inferred from the depth distribution of the average *b*-values shown in Fig. 5c obtained in (Popandopulo and Lukk, 2014). Here again, three horizons are distinguished. The top horizon with an average *b*-value of 0.82 covers the depth interval from 0 to 9 km. The middle horizon where the average *b*-value is 0.78 corresponds to the depths from 10 to 16 km. Finally, the bottom horizon is located below a depth of 16 km, and the *b*-value in this horizon is 1.2. In the cited work, the depth behavior of the *b*-value was interpreted from the standpoint of the hypothesis suggesting the existence of a brittle–ductile transition (BDT) zone in the Earth's crust (Dragoni, 1993; Amitrano, 2003; Jin et al., 2004; Gueydan et al., 2004; Doglioni et al., 2010; Dinkelman et al., 2010; Daub et al., 2011; Spada et al., 2013; Schoulz, 2015). According to this hypothesis, the state of the crustal material along the depth is mainly determined by the lithostatic pressure and temperature. As a result of the interplay between these two factors, the strength of a brittle material increases with depth due to an increase in the confining pressure, whereas the ductile strength of the material decreases with an increase in temperature. It is hypothesized that the BDT zone itself is characterized by high strength of crustal material and accommodates the most severe earthquakes. Typically, the bottom of the BDT zone corresponds to the lower boundary of the seismogenic layer in the upper part of the brittle crust within the depths of 15–16 km. The region between the middle and bottom horizons in the crust (~16–18 km) is marked by a sharply weakening seismicity level due to the presence of the phase transition zone from the elastic brittle to the plastic state of the crustal material. At the large depths below 15–16 km, the conditions for the intense accumulation of elastic stresses and their release in the form of the strong seismic events are absent. This situation emerges because of the enhancement of yielding properties (plasticity) of the material at these depths.

From this standpoint, it is possible to explain the uniform type of the time variations in *b*-value observed in the different layers of the crust. Under the change in the tectonic stresses, the upper brittle horizons of the Earth's crust in the depth interval of ~0–9 km can be assumed to behave as a single elastic layer. Moreover, the differences in the amplitude of the time variations in *b*-value arise in the consolidation zone in the sources of the future strong earthquakes. The intermediate zone at the depths of 10–16 km includes the BDT zone where the medium has more rigid properties. Here, the response of the medium to the changes in the tectonic stresses somewhat differs from that in the overlying layer. Finally, the lower layer, due to a sharp increase in the plasticity of the crustal material weakly interacts with the upper BDT layer, and the small fluctuations in the tectonic stresses cause relatively strong variations in the *b*-value. The division of the Earth's crust in this local area of the sample into the three layers could also be performed based on the analysis of the range of variability of the time series presented in Table 1. It can be seen that the variability of the time series in the upper layer for the first four horizons varies within 9%. The variability sharply increases to 14% in the intermediate horizons (nos. 5 and 6, Table 1) and has a significant jump to 24% in the lower horizons,.

Interestingly, at approximately the same depths, three horizons were also identified in the study of the focal mechanisms of the Garm earthquakes where these horizons sharply differ in terms of the type of the deformation state of the Earth's crust (Lukk, 2011).

The existence of the BDT zone can also explain the sharp decrease in the minimum *MPE* and the increase in the variability of the *b*-value time series below a depth of 16 km (Table 1 and Figs. 4 and 5c). Due to the fact that below the BDT zone, the state of the medium sharply changes from brittle to ductile, the Earth's crust at the large depths exceeding 16 km is mainly

plastic. At the same time, the high-density inhomogeneities penetrate to the lower crust and, therefore, at these depths, rigid structural blocks are preserved within which a certain fraction of tectonic stresses can be accumulated and then released by the earthquakes with the magnitudes corresponding to the sizes of these blocks. It is most likely that the largest solid (not melted) structural blocks at these depths have the sizes corresponding to the minimum *MPE*. It can be hypothesized that the gaps between these rigid structural blocks are abundantly filled with ductile material containing the inclusions of smaller structural blocks, which is reflected in the shape of the FMD of the earthquakes. Under the change of tectonic stresses at these depths, this state of the medium leads to a relatively large variability of the GR *b*-value. As a result, we see that the range Δb of the variations in the GR *b*-value in the lower crustal layers reaches 1.2, i.e. the amplitude of the curves of the *b*-value varies within 0.8 to 2.0.

At the same time, the variability of the *b*-value curves at these depths can be associated with the influence of purely technical (methodological) factors. The magnitude range of the earthquakes included in the sample of earthquake data for constructing the FMD at these depths is $\Delta M = 2$ and varies within 1 to 3, which is, to some extent, insufficient for reliable estimating of *b*-value (Marzocchi and Sandri, 2004; Sandri and Marzocchi, 2007). According to the cited works, the minimum range of the magnitudes required for reliable estimating the *b*-value is at least 2.5. Hence, one may suppose that the determination of *b*-value at these depths raises certain doubts. However, the similarity of the pattern of *b*-value variations before the earthquakes with $M \geq MPE$ at these depths with the behavior of the curves for the upper horizons suggests that the character of the observed process of preparation of a "strong" earthquake is similar for all the studied depth intervals, i.e. it has a property of self-similarity and, hence, reflects the physics of the process at these depths.

And finally, the differentiated analysis of the time variations in the *b*-value in the different depth intervals has shown that the probability of successful predicting a medium-term estimate of the time period for the occurrence of a "strong" earthquake with $M \geq MPE$ can be higher than 71%. The studies have shown that the time anomalies in the *b*-value are localized in the vicinity of the hypocenter of a future earthquake. The statistics obtained by the analysis of 18 earthquakes with $M \geq MPE$ that occurred at different depths indicates that the results are reliable and physically meaningful. Based on this, we may conclude that the used approach is very promising for estimating the depth of a predicted earthquake.

CONCLUSIONS

The detailed studies of spatiotemporal variations in the Gutenberg–Richter *b*-value depending on the depth and lateral position of the sample of the earthquakes in the Earth's crust are conducted for the Garm region, Tajikistan.

The parameter of the minimum magnitude of a predicted earthquake (*MPE*) determined from the rightmost segment of the linear part of the Gutenberg–Richter relationship is studied across the area and along the depth. It is shown that this parameter is a characteristic of the structural crustal blocks and varies both areally and along the depth.

The quality assessment of earthquakes' prediction based on 38 "strong" earthquakes with $M \geq MPE$ that occurred in seven local regions during a 23-year observation period by the FastBee algorithm (Papadopoulos and Baskoutas, 2009) shows that the emergence of the *b*-value anomalies is accompanied in 84% of cases by a successful prediction. At the same time, the overall assessment of the probability of a medium-term prediction of "strong" earthquakes, with false alarms and missed events taken into account, is 71%.

The time variations in the *b*-value in the different depth intervals show that in the vast majority of cases, the earthquakes with magnitudes $M \geq MPE$ are preceded by the significant time anomalies in the *b*-value in the vicinity of the hypocenters of these events. Moreover, the maximum amplitudes of these anomalies are concentrated closely around the seismic source and decay with distance from the source. The observed time anomalies in the *b*-value have a positive bay-like shape and are not accidental which follows from their sufficient statistical representativeness (18 events with $M \geq MPE$). It is shown that the quality of forecasting the "strong" earthquakes with $M \geq MPE$ can be significantly improved by differentiated monitoring of time variations of *b*-value separately in the different depth intervals. It is concluded that with this approach it will be also possible to estimate the source depth of a future strong earthquake.

It is hypothesized that the front of the deformation waves appearing on certain time intervals in the neighboring local regions of the spatial sample of the earthquakes is detected. The supposed deformation waves move with a rate of 40–50 km/yr with the propagation direction of the wavefront from NE to SW.

The results of the study can be used for medium-term forecasting the "strong" earthquakes with $M \geq MPE$, for estimating the depth of the forecast earthquake and for the assessment of overall seismic hazard in the seismically active regions.

REFERENCES

Aki, K., Maximum likelihood estimate of b in the formula $\log N = a - bM$ and its confidence limits, *Bull. Earthquake Res. Inst., Univ. Tokyo*, 1965, vol. 43, pp. 237–239.

Amitrano, D., Brittle_ductile transition and associated seismicity: Experimental and numerical studies and relationship with the *b* value, *J. Geophys. Res.*, 2003, vol. 108, no. B1, p. 2044.
https://doi.org/10.1029/2001JB000680

Baskoutas, I. and Popandopoulos, G., Qualitative precursory pattern before several strong earthquakes in Greece, *Res. Geophys.*, 2014, vol. 4, pp.7–11. https://doi.org/10.4081/rg.2014.4899

Bath, M., *Spectral Analysis in Geophysics*, Amsterdam: Elsevier, 1974.

Bykov, V.G., Strain waves in the Earth: theory, field data, and models, *Russ. Geol. Geophys.*, 2005, no. 11, pp. 1158–1170.

Daub, E.G., Shelly, D.R., Guyer, R.A., and Johnson, P.A., Brittle and ductile friction and the physics of tectonic tremor, *Geophys. Res. Lett.*, 2011, vol. 38, Paper ID L10301. https://doi.org/10.1029/2011GL046866

Dinkelman, M.G., Granath, J., Bird, D., Helwig, J., Kumar, N., and Emmet, P., Predicting the Brittle_Ductile (B_D) Transition in Continental Crust Through Deep, Long Offset, Prestack Depth Migrated (PSDM), 2D Seismic Data, *Search Discovery Artic.*, 2010, no. 40511.

Dobrovol'skii, I.P., Earthquake preparation. Deformations and the size of the zone of manifestation of the precursors, in *Eksperimental'naya seismologiya* (Experimental Seismology), Moscow: Nauka, 1983, pp. 17–25.

Dobrovol'skii, I.P., *Teoriya podgotovki tektonicheskogo zemletryaseniya* (Theory of Preparation of a Tectonic Earthquake), Moscow: IFZ AN SSSR, 1991.

Doglioni, C., Barba, S., Carminati, E., and Riguzzi, F., Role of the brittle–ductile transition on fault activation, *Phys. Earth Planet. Inter.,* 2010, vol. 184, nos. 3–4, pp. 160–171.

Dragoni, M., The brittle-ductile transition in tectonic boundary zones, *Ann. Geofis.*, 1993, vol. 36, no. 2, pp. 37–44.

Gerstenberger, M.C., Wiemer, S., Giardini, D., Hauksson, E., and Jones, L.M., Time-dependent hazard assessment for California in near real-time, *Seismol. Res. Lett.*, 2001b, vol. 72, p. 273.

Gomberg, J., Seismicity and detection/location threshold in the southern Great Basin seismic network, *J. Geophys. Res.*, 1991, vol. 96, no. B10, pp.16,401–16,414.

Gueydan, F., Leroy, Y.M., and Jolivet, L., Mechanics of low_angle extensional shear zones at the brittle–ductile transition, *J. Geophys. Res.*, 2004, vol. 109, Paper ID B12407. https://doi.org/10.1029/2003JB002806

Gutenberg, B. and Richter, Ch.F., Frequency of earthquakes in California, *Bull. Seismol. Soc. Am.*, 1944, vol. 34, pp. 185–188.

Hamburger, M.W., Sarewitz, D.E., Pavlis, G.L., and Popandopulos, G.A., Structural and seismic evidance for intracontinental subduction in the Peter the First Range, Soviet Central Asia, *Geol. Soc. Am. Bull.*, 1992, vol. 104, pp. 397–408.

Ishimoto, M. and Iida, K., Observations of earthquakes registered with the microseismograph constructed recently, *Bull. Earthquake Res. Inst., Univ. Tokyo*, 1939, vol. 17, pp. 443–478.

Jin, A., Aki, K., Liu, Z., and Keilis-Borok, V.I., Seismological evidence for the brittle ductile interaction hypothesis on earthquake loading, *Earth Planets Space*, 2004, vol. 56, pp. 823–830.

Kasahara, K., *Earthguake Mechanics*, Cambriage: Cambriage Univ. Prress, 1981.

Kijko, A. and Sellevoll, M.A., Estimation of Earthquake Hazard Parameters from Incomplete Data Files. 2. Incorporation of Magnitude Heterogeneity, *Bull. Seismol. Soc. Am.*, 1992. vol. 82, no. 1, pp. 120–134.

Kostrov, B.V. and Das, S., *Principles of Earthquake Source Mechanics*, Cambridge: Cambridge Univ. Press, 1988.

Lukk, A.A. and Popandopoulos, G.A., Reliability of determining the parameters of Gutenberg–Richter distribution for weak earthquakes in Garm, Tajikistan, *Izv., Phys. Solid Earth*, 2012, vol. 48, nos. 9–10, pp. 698–720.

Lukk, A.A. and Shevchenko, V.I., Structure of seismic field and fault tectonics of the Garm region in Tajikistan, *Izv. Akad. Nauk SSSR, Fiz. Zemli*, 1990, no. 1, pp. 5–20.

Main, I.G., Meredith, P.G., and Sammonds, P.R., Temporal variations in seismic event rate and *b*-values from stress corrosion constitutive laws, *Tectonophysics*, 1992, vol. 211, pp. 233–246.

Marzocchi, W. and Sandri, L., A review and new insights on the estimation of the *b*-value and its uncertainty, *Ann. Geophys.*, 2003, vol.46, no. 6, pp. 1271–1282.

Mignan, A. and Woessner, J. *Completeness magnitude in earthquake catalogs.* Community Online Resource for Statistical Seismicity Analysis. 2012. https://doi.org/10.5078/corssa-00180805

Mogi, K., Study of the elastic shocks caused by the fracture of heterogeneous materials and its relation to earthquake phenomena, *Bull. Earthquake Res. Inst., Univ. Tokyo*, 1962, vol. 40, pp. 125–173.

Mori, J. and Abercrombie, R.E., Depth dependence of earthquake frequency-magnitude distributions in California: implications for the rupture initiation, *J. Geophys. Res.*, 1997, vol. 102, pp. 15081–15090.

Myachkin, V.I., Kostrov, B.V., Sobolev, G.A., and Shamina, O.G., Basic physics of the source and earthquake precursors, in *Fizika ochaga zemletryaseniya* (Physics of an Earthquake Source), Moscow: Nauka, 1975, pp. 6–29.

Nersesov, I.L. and Popandopoulos, G.A., Spatial heterogeneity of temporal variations in the velocity parameters in the Earth's crust of the Garm region, *Izv. Akad. Nauk SSSR, Fiz. Zemli*, 1988, no. 8, pp. 13–24.

Nikolaevskiy, V.N., *Geomechanics and Fluid Dynamics*, Dordecht: Kluwer, 1996.

Popandopoulos, G.A., Determining the coordinates of the hypocenters of local earthquakes at the Garm Geophysical Test Site, in *Zemletryaseniya i protsessy ikh podgotovki* (Earthquakes and the Processes of Their Preparation), Moscow: Nauka, 1991, pp. 5–23.

Popandopoulos, G.A., Detailed study of time variations in the Gutenberg–Richter *b*-value based on highly accurate seismic observations at the Garm prognostic site, Tajikistan, *Izv., Phys. Solid Earth*, 2018, vol. 54, no. 4, pp. 612–631.

Papadopoulos, G.A. and Baskoutas, I.G., New tool for the temporal variation analysis of seismic parameters, *Nat. Hazards Earth Syst. Sci.,* 2009, vol. 9, pp. 859–864. www.nat-hazards-earth-syst-sci.net/9/859/2009.

Popandopoulos, G.A. and Baskoutas, I., Regularities in the time variations of seismic parameters and their implications for prediction of strong earthquakes in Greece, *Izv., Phys. Solid Earth*, 2011, vol. 47, no. 11, pp. 974–994.

Popandopoulos, G.A. and Chatziioannou, E., Gutenberg-Richter Law Parameters Analysis Using the Hellenic Unified Seismic Network Data Through FastBee Technique, *Earth Sci.*, 2014, vol. 3, no. 5, pp. 122–131. https://doi.org/10.11648/jearth.20140305.12

Popandopoulos, G.A. and Lukk, A.A., The depth variations in the *b*-value of frequency–magnitude distribution of the earthquakes in the Garm region of Tajikistan, *Izv., Phys. Solid Earth*, 2014, vol. 50, no. 2, pp. 273–288.

Popandopoulos, G.A. and Nersesov, I.L., Some results of the analysis of 30-year time series of valocity parameters at the Garm geodynamical testing site, in *Zemletryaseniya i protsessy ikh podgotovki* (Earthquakes and the Processes of Their Preparation), Moscow: Nauka, 1991, pp. 139–152.

Popandopoulos, G.A., Baskoutas, I., and Chatziioannou, E., The spatiotemporal analysis of the minimum magnitude of completeness *Mc* and the Gutenberg–Richter *b*-value using the earthquake catalog of Greece, *Izv., Phys. Solid Earth*, 2016, vol. 52, no. 2, pp. 195–209.

Ruff, L., Asperity distributions and large earthquake occurrence in subduction zones, *Tectonophysics*, 1992, vol. 211, pp. 61–83.

Rydelek, P.A. and Sacks, I.S., Testing the completeness of earthquake catalogs and the hypothesis of self-similarity, *Nature*, 1989, vol. 337, pp. 251–253.

Sadovskii, M.A. and Pisarenko, V.F., *Seismicheskii protsess v blokovoi srede* (Seismic Process in a Block Medium), Moscow: Nauka, 1991.

Sandri, L. and Marzocchi, W., A technical note on the bias in the estimation of the *b*-value and its uncertainty through the Least Squares technique, *Ann. Geophys.*, 2007, vol. 50, no. 3. pp. 329–339.

Scholz, C.H., The frequency-magnitude relation of microfracturing in rock and its relation to earthquakes, *Bull. Seismol. Soc. Am.,* 1968, vol. 58, pp. 399–415.

Scholz, C.H., On the stress dependence of the earthquake b value, *Geophys. Res. Lett.*, 2015, vol. 42, pp.1399–1402. https://doi.org/10.1002/2014GL062863

Schorlemmer, D., Wiemer, S., and Wyss, M., Earthquake statistics at Park field: 1. Stationarity of *b*-values, *J. Geophys. Res.*, 2004a, vol. B12307. https://doi.org/10.1029/2004JB003234

Schorlemmer, D., Wiemer, S., Wyss, M., and Jackson, D.D., Earthquake statistics at Park field: 2. Probabilistic forecasting and testing, *J. Geophys. Res.*, 2004b, vol. B12307. https://doi.org/10.1029/2004JB003234

Schorlemmer, D., Wiemer, S., and Wyss, M., Variations in earthquake-size distribution across different stress regimes, *Nature*, 2005, vol. 437, pp. 539–542. https://doi.org/10.1038/nature04094

Sherman, S.I., Deformation waves as a trigger mechanism of seismic activity in seismic zones of the continental lithosphere, *Geodinam. Tektonofiz.*, 2018, vol. 4, no. 2, pp. 83–117.

Shi, Y. and Bolt, B.A., The standard error of the Magnitude-frequency *b* value, *Bull. Seismol. Soc. Am.*, 1982, vol. 72, pp. 1677–1687.

Smirnov, V.B., Earthquake catalogs: evaluation of data completeness, *Volcanol. Seismol.*, 1998, vol. 19, pp. 497–510.

Sobolev, G.A., *Osnovy prognoza zemletryasenii* (Basics of Earthquake Prediction), Moscow: Nauka, 1993.

Spada, M., Tormann, T., Wiemer, S., and Enescu, B., Generic dependence of the frequency-size distribution of earthquakes on depth and its relation to the strength profile of the crust, *Geophys. Res. Lett.*, 2013, vol. 40, pp. 709–714. https://doi.org/10.1029/2012GL054198

Turcotte, D.L. and Schubert, G., *Geodynamics*, New York: Wiley, 1982.

Wiemer, S., A software package to analyze seismicity: ZMAP, *Seismol. Res. Lett.*, 2001, vol. 72, no. 3, pp. 373–382.

Wiemer, S. and Wyss, M., Mapping the frequency-magnitude distribution in asperities: An improved technique to calculate recurrence times?, *J. Geophys. Res.*, 1997, vol. 102, pp. 15,115–15,128.

Wiemer, S. and Wyss, M., Minimum magnitude of completeness in earthquake catalogs: Examples from Alaska, the western United States and Japan, *Bull. Seismol. Soc. Am.*, 2000, vol. 90, no. 4, pp. 859–869.

Wiemer, S. and Wyss, M., Mapping spatial variability of the frequency—magnitude distribution of earthquakes, *Adv. Geophys.*, 2002, vol. 5, pp. 259–302.

Woessner, J. and Wiemer, S., Assessing the quality of earthquake catalogues: Estimating the magnitude of completeness and its uncertainty, *Bull. Seismol. Soc. Am.*, 2005, vol. 95, pp. 684–698.

Wyss, M. and Stefansson, R., Nucleation points of recent main shocks in southern Iceland mapped by *b*-values, *Bull. Seismol. Soc. Am.*, 2006, vol. 96, pp. 599–608.

Wyss, M., Hasegawa, A., and Nakajima, J., Source and path of magma for volcanoes in the subduction of northeastern Japan, *Geophys. Res. Lett.*, 2001a, vol. 28, pp.1819–1822.

Wyss, M., Pacchiani, F., Deschamps, A., and Patau, G., Mean magnitude variations of earthquakes as a function of depth: different crustal stress distribution depending on tectonic setting, *Geophys. Res. Lett.*, 2008, vol. 35, Paper ID L01307. https://doi.org/10.1029/2007GL031057

Zheng, B., Hamburger, M.W., and Popandopulos, G.A., Precursory seismicity changes preceding moderate and large earthquakes in the Garm region, Central Asia, *Bull. Seismol. Soc. Am.*, 1995, vol. 85, pp. 571–589.

Zhu, A., Xu, X., Hu, P., Zhou, Y., Chen, G., and Gan, W., Variation of b value with hypocentral depth in Beijing area: Implications for earthquake nucleation, *Chin. Sci. Bull.*, 2005, vol. 50, no. 7, pp.691–695.

Translated by M. Nazarenko